Supporting Information

Fused Metalloporphyrin Thin Film with Tunable Porosity via Chemical Vapor Deposition

Kamal Baba, Giuseppe Bengasi, François Loyer, Joao Paulo Cosas Fernandes, Dana El Assad, Olivier De Castro, Nicolas D. Boscher*

Materials Research and Technology Department, Luxembourg Institute of Science and Technology, 5 Avenue des Hauts-Fourneaux, L-4362 Esch-sur-Alzette, Luxembourg

Corresponding author: nicolas.boscher@list.lu

Table of content

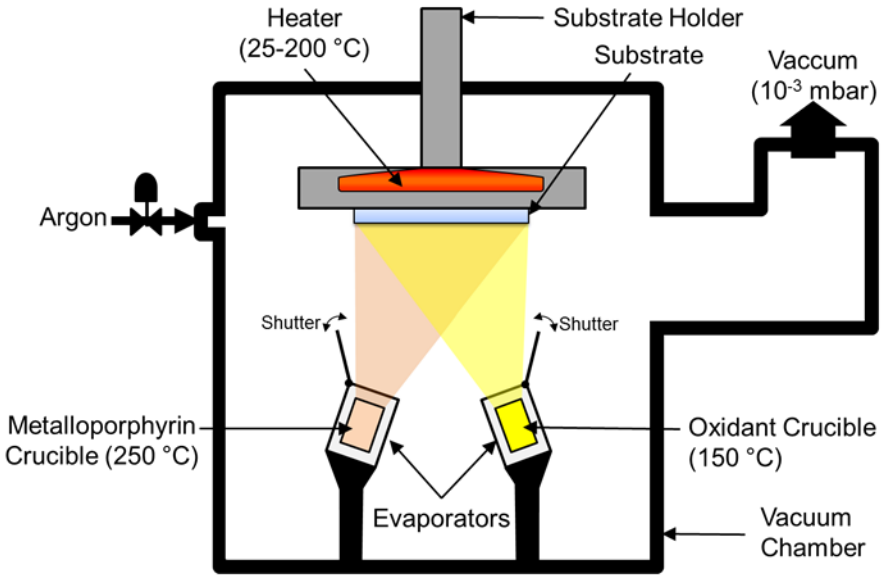

Scheme S1. Scheme of the oxidative chemical vapour deposition (oCVD) reactor for the deposition of conjugated porphyrins using $FeCl_3$ oxidant.

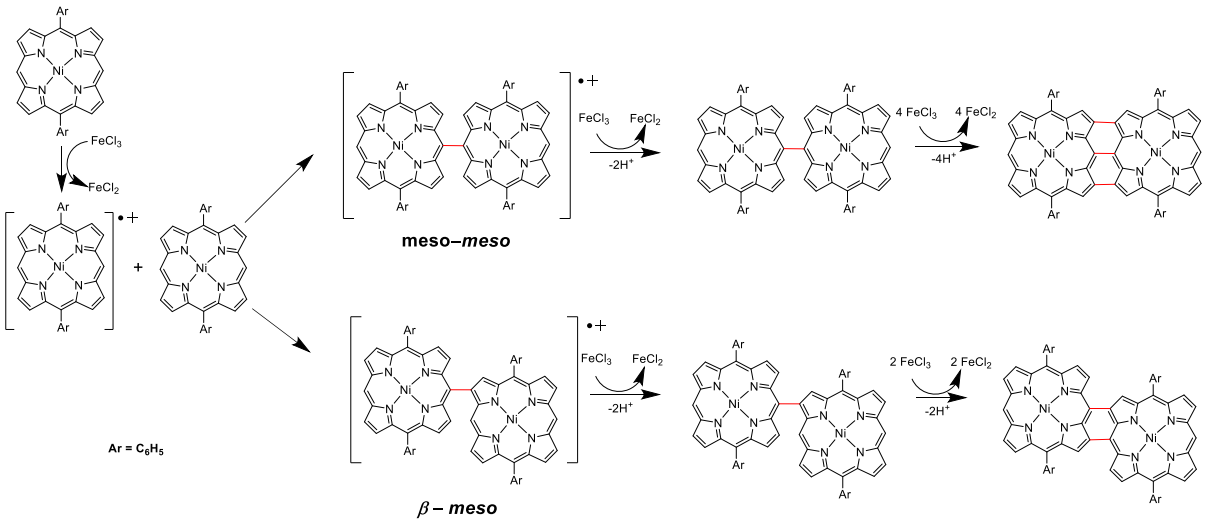

Scheme S2. Reaction scheme for the formation of triply and doubly linked porphyrin tapes in oCVD using $FeCl_3$ act as oxidant.

Table S1. Oxidative chemical vapour deposition (oCVD) reaction conditions.

Sample name	**Reference**	**25**	**50**	**100**	**150**	**200**
Monomer	Nickel(II) 5,15-(diphenyl)porphyrin					
Chemical formula	$C_{32}H_{20}N_4Ni$					
Molecular weight ($g \cdot mol^{-1}$)	519,23					
Sublimation temperature (°C)	250					
Sublimated amount (mg)	8.3	5.5	9.5	8.9	7.7	8.8
Sublimated amount (µmol)	15.9	10.6	18.3	17.1	14.8	16.9
Oxidant	-	Iron(III) chloride				
Chemical formula		$FeCl_3$				
Molecular weight ($g \cdot mol^{-1}$)		160.84				
Sublimation temperature (°C)		150				
Sublimated amount (mg)		97.1	109.9	93.7	103.4	67.7
Sublimated amount (µmol)		603.7	683.3	582.6	642.9	420.9
Substrate temperature (°C)	150	25	50	100	150	200
Deposition time (min)	30					

Table S2. Thickness, weight per unit area, density, conductivity, average roughness (Ra), modulus, water contact angle (WCA) and water uptake for the reference and oCVD thin films.

Sample name	**Reference**	**25**	**50**	**100**	**150**	**200**
Thickness (nm)	52 ± 5	60 ±5	130 ± 15	345 ±22	600 ± 72	1160 ± 105
Weight per unit area ($\mu g \cdot cm^{-2}$)	27.5 ± 14	29.1 ± 5	30.1 ± 11	24.4 ± 8	24.2 ± 7	26.2 ± 11
Density ($g \cdot cm^{-3}$)	4.7 ± 2.4	4.8 ± 0.8	2.3 ± 0.8	0.7 ± 0.2	0.4 ± 0.1	0.2 ± 0.1
Conductivity (10^{-3} S cm^{-1})	ca. 10^{-8}-10^{-9}	$1.5 \cdot 10^{-3}$	$14.2 \cdot 10^{-3}$	$9.6 \cdot 10^{-3}$	$22.4 \cdot 10^{-3}$	$6.3 \cdot 10^{-3}$
Roughness (nm)	-	1.2 ± 0.4	2.5 ± 0.5	2.6 ± 0.6	3.5 ± 0.2	6.7 ± 0.9
Modulus (GPa)	-	5.4 ± 0.9	2.7 ± 0.2	1.9 ± 0.3	2.2 ± 0.1	2.4 ± 0.3
WCA (°)	84.0 ± 2	86.7 ± 3	101.2 ± 3	96..8 ± 3	104.6 ± 2	101.3 ± 4
Water uptake per surface unit ($\mu g \cdot cm^{-2}$)	28.9 ± 7.7	21.1 ± 6.4	26.1 ± 19.7	32.8 ± 9	88.2 ± 35.8	113.7 ± 45.5

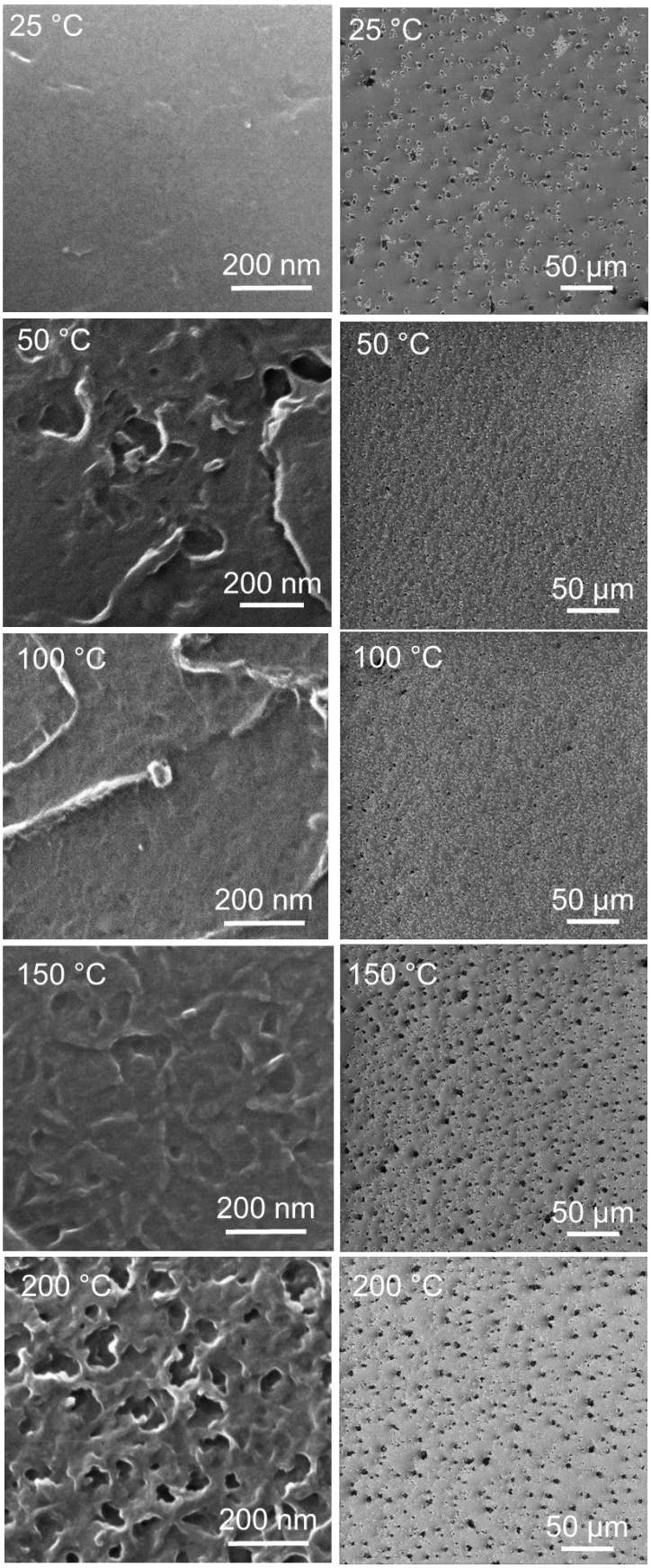

Figure S1. High (left) and low (right) magnification helium ion microscopy (HIM) top view images of the oCVD thin films deposited at different substrate temperature.

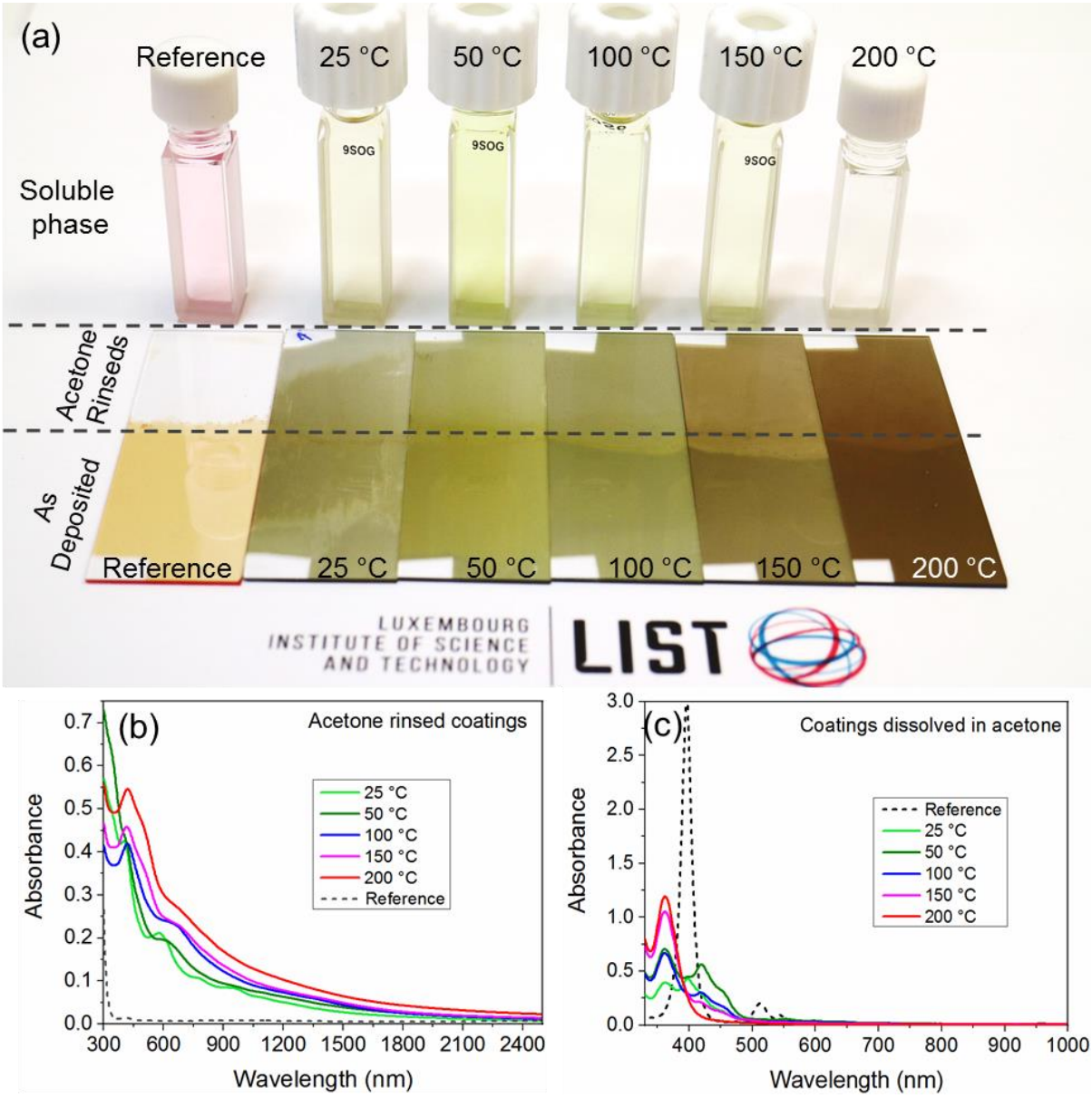

Figure S2. (a) Optical image of reference and oCVD thin films as-deposited (bottom half of the microscope glass slides), acetone rinsed (upper half) and their soluble phase in acetone (cuvettes). UV/Vis/NIR spectra of (b) the reference and oCVD thin films deposited on microscope glass slides and rinsed with acetone and (c) soluble phase of the reference and oCVD thin films in acetone.

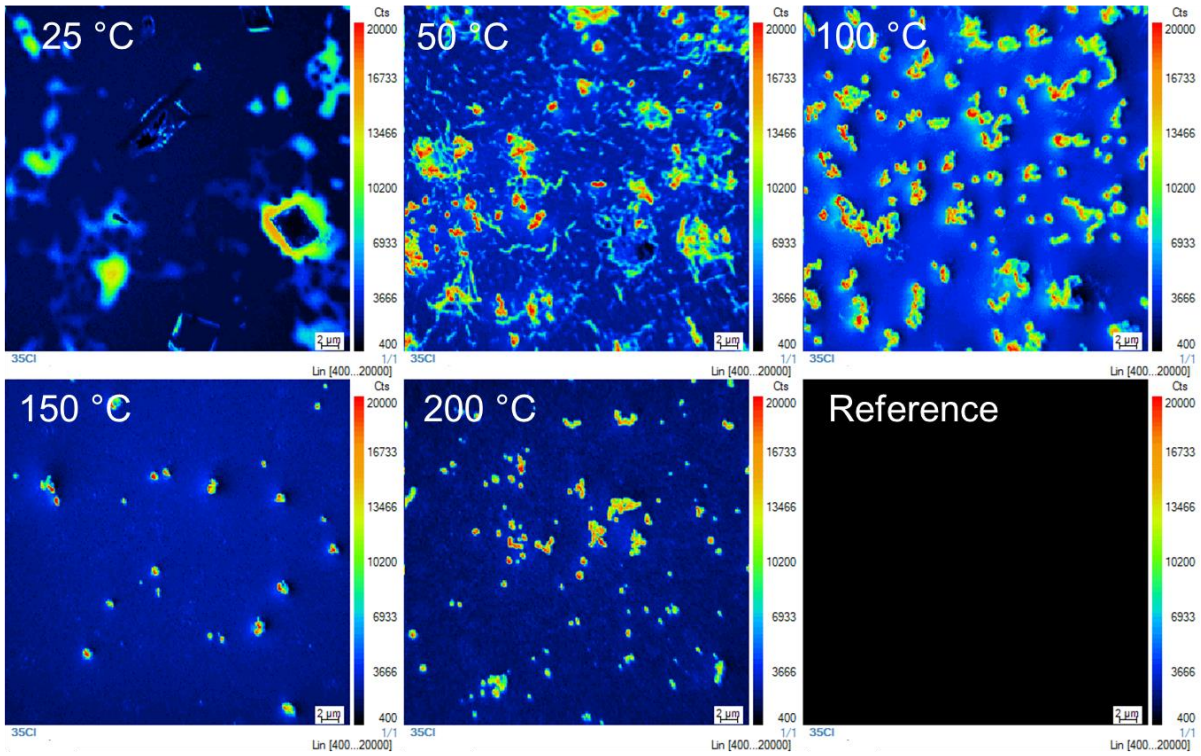

Figure S3. NanoSIMS elemental distribution of ^{35}Cl images on a reference thin film and the oCVD thin films deposited at 25°C, 50°C, 100°C, 150°C and 200°C. Field of view is 40 × 40 µm and counts scale is 400-20000 counts.

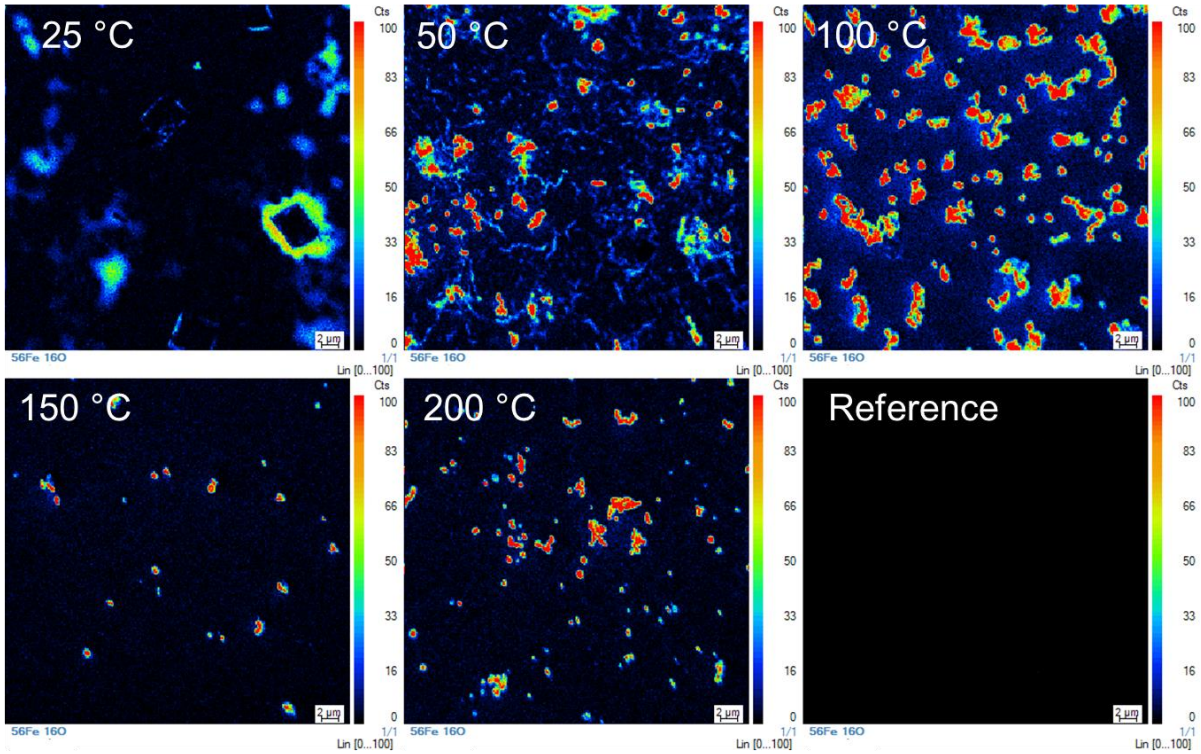

Figure S4. NanoSIMS elemental distribution of $^{56}Fe^{16}O$ images on a reference thin film and the oCVD thin films deposited at 25°C, 50°C, 100°C, 150°C and 200°C. Field of view is 40 × 40 µm and counts scale is 0-100 counts.

Table S3. Relative atomic concentration of the oCVD thin films and theoretical composition of NiDPP and fused NiDPP oligomers.

% Substrate temperature (°C)	C 1s	N 1s	Ni 2p	Fe 2p	Cl 2p
25	86.7	5.9	1.4	3.5	2.5
50	87.7	6.0	0.8	3.1	2.4
100	87.0	5.5	1.2	3.7	2.5
150	89.1	5.1	1.0	2.8	2.0
200	87.0	6.3	1.5	2.6	2.5
NiDPP	86.5	10.8	2.7	-	-

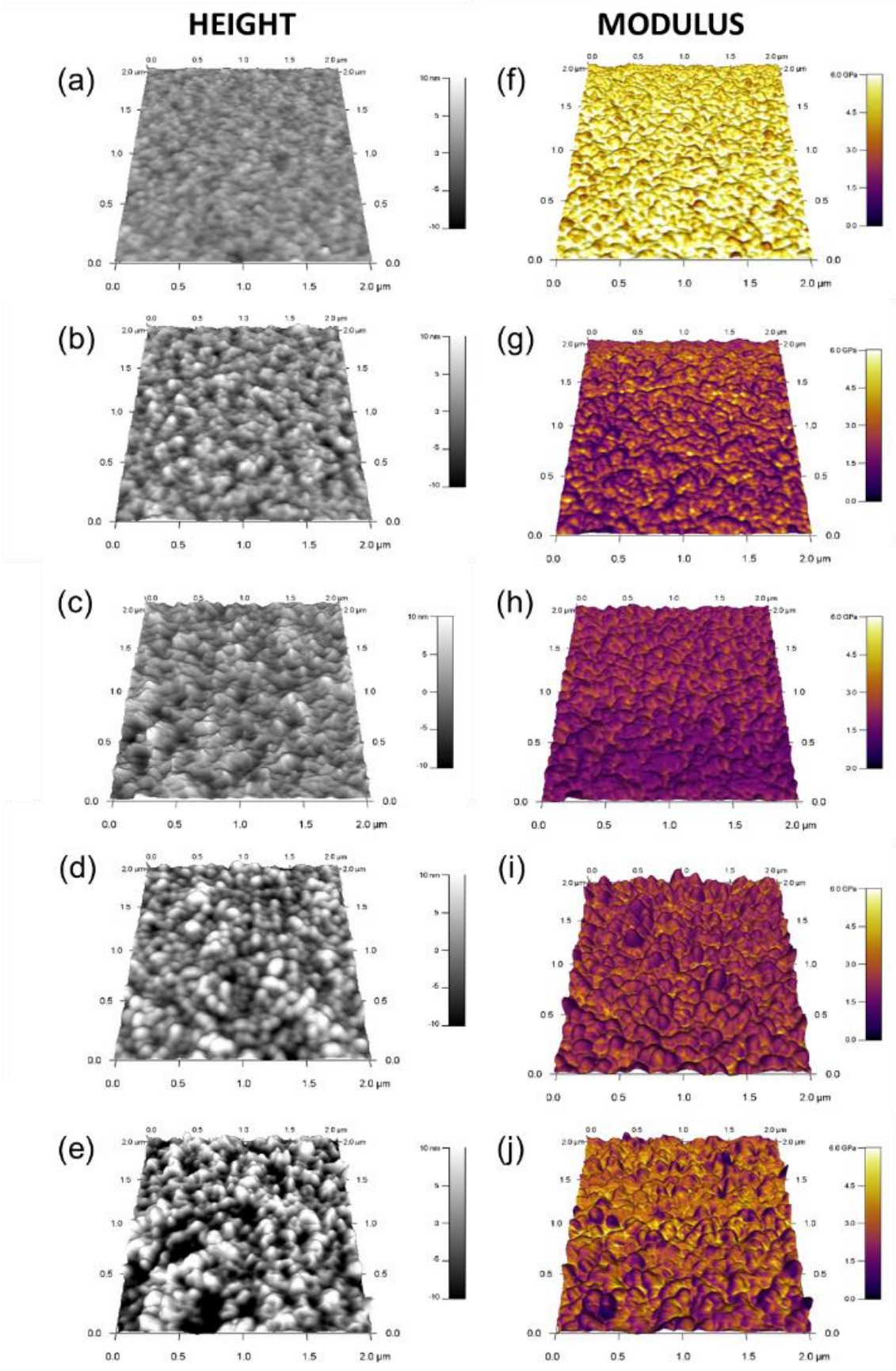

Figure S5. (a-e) Height and (f-j) Modulus AFM images of the oCVD thin films elaborated at (a & f) 25°C, (b & g) 50°C, (c & h) 100°C, (d & i) 150°C and (e & j) 200°C.

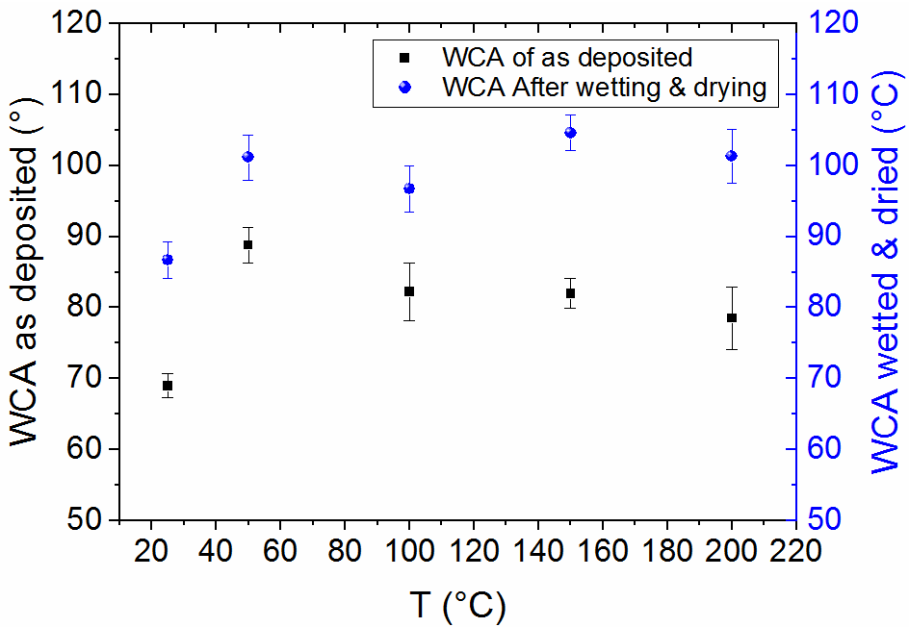

Figure S6. Water contact angle (WCA) of the as-deposited oCVD thin films before and after rinsing with water and dried at 70°C under vacuum for 12 hours.

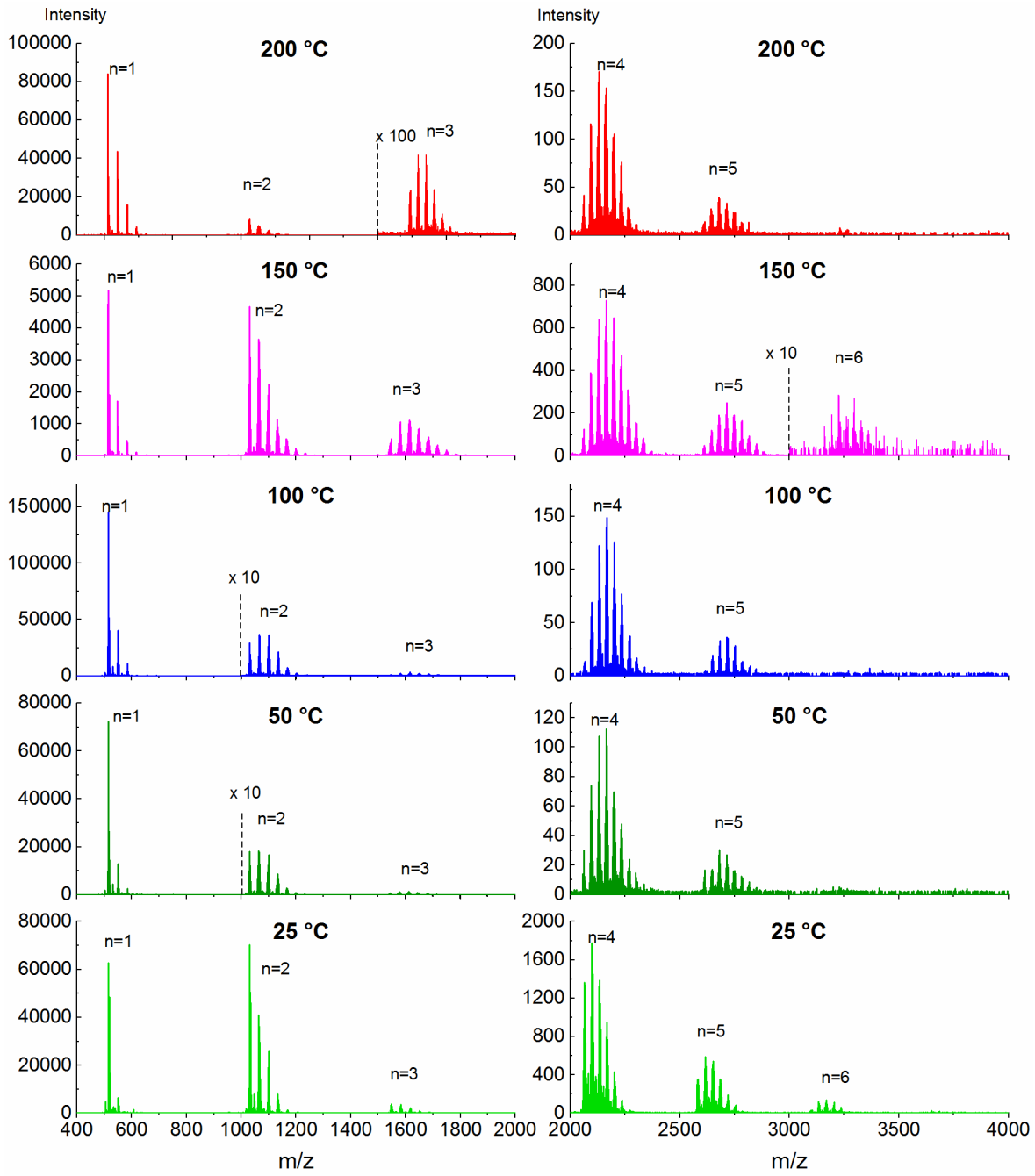

Figure S7. AP-LDI-HRMS spectra of the oCVD thin films elaborated at different substrate temperatures. Ions are detected as radical cations $[M]^{\bullet+}$. Two scan events were used to acquire spectra within a broad mass range (m/z 400–2000 and m/z 2000–4000). One should note that instrumental limit is m/z 4000. Moreover, AP-LDI-HRMS does not provide a complete representation of all the oligomer/polymer chains formed since the ionization and desorption of larger molecules are far less probable, making their detection more challenging.

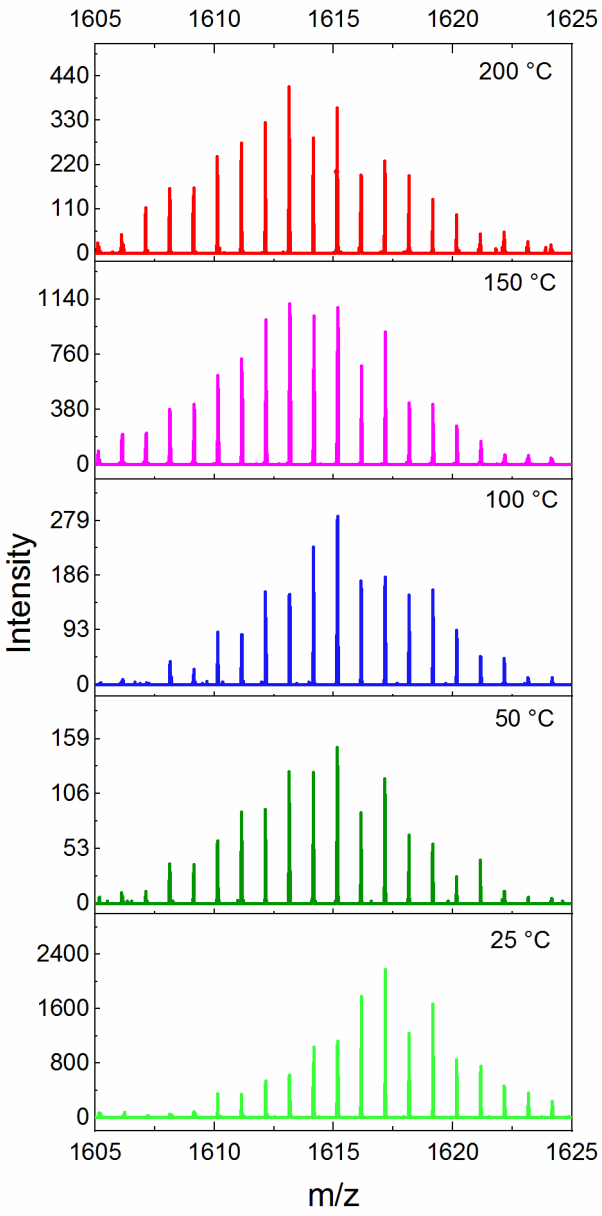

Figure S8. Trimer region of the AP-LDI-HRMS spectra in the mass range m/z 1605 to 1625 of the oCVD thin films elaborated at different substrate temperatures.

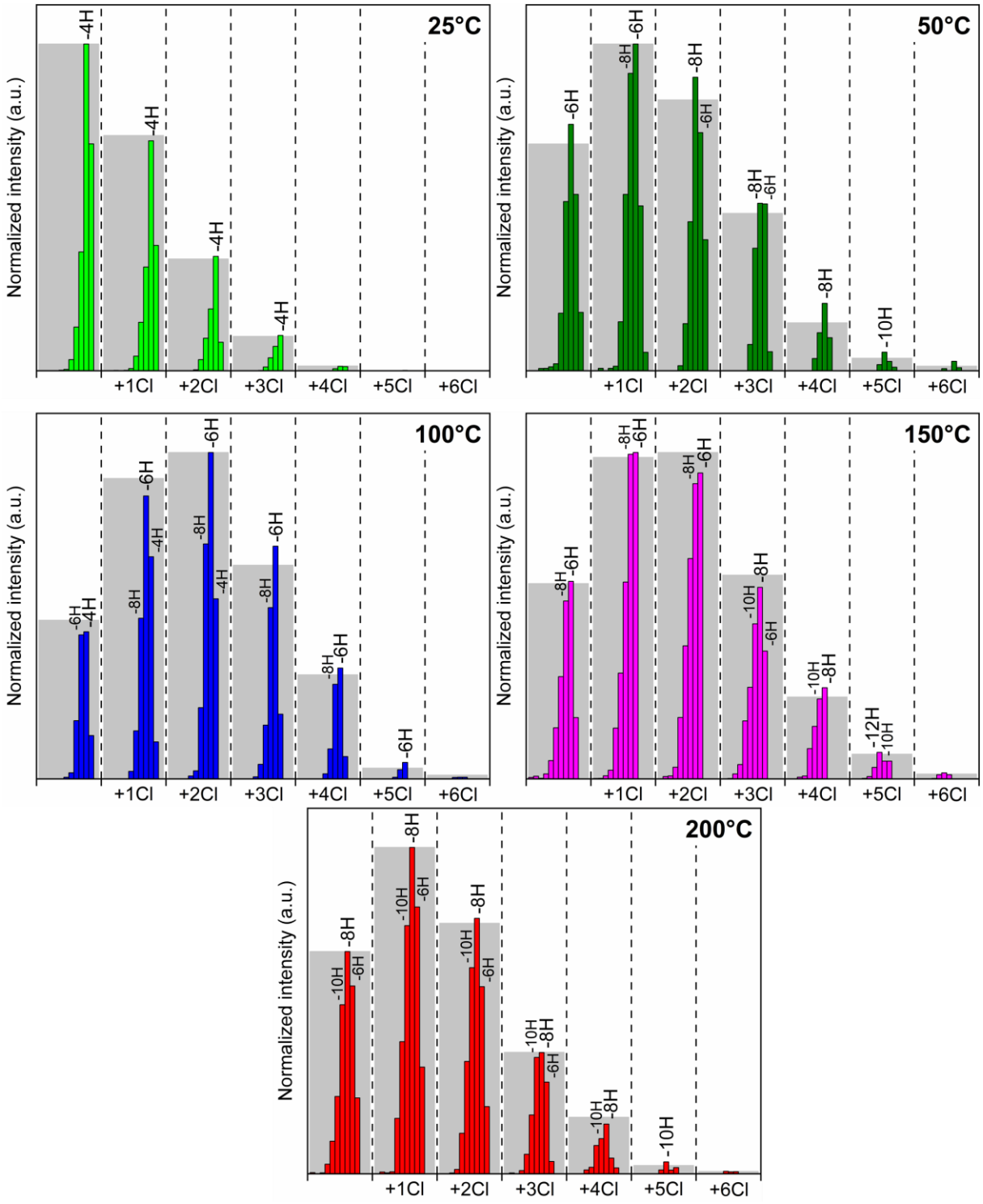

Figure S9. Relative abundance of the different trimeric species $[(NiDPP)_3 –(H_2)_n + (Cl - H)_m]^+$ detected by high resolution mass spectrometry for the oCVD thin films deposited at 25°C, 50°C, 100°C, 150°C and 200°C. Such a presentation of the AP-LDI-HRMS data enables a better overview of the ($-H_2$) pairs evolution, which cannot be readily observed from the AP-LDI-HRMS spectra due to the large distribution of chlorinated species and the isotopic patterns.

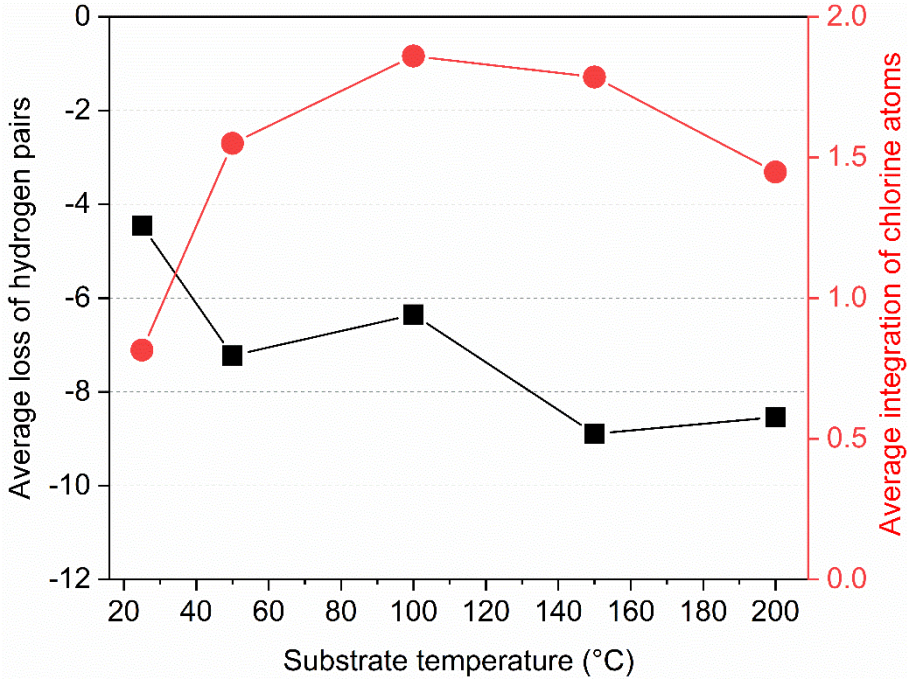

Figure S10. Evolution as a function of the reaction temperature of the average numbers of hydrogen atoms eliminated (-2H, black) and chlorine atoms integrated (+Cl -H, red) on the trimeric $NiDPP_3$ species detected by high resolution mass spectrometry.

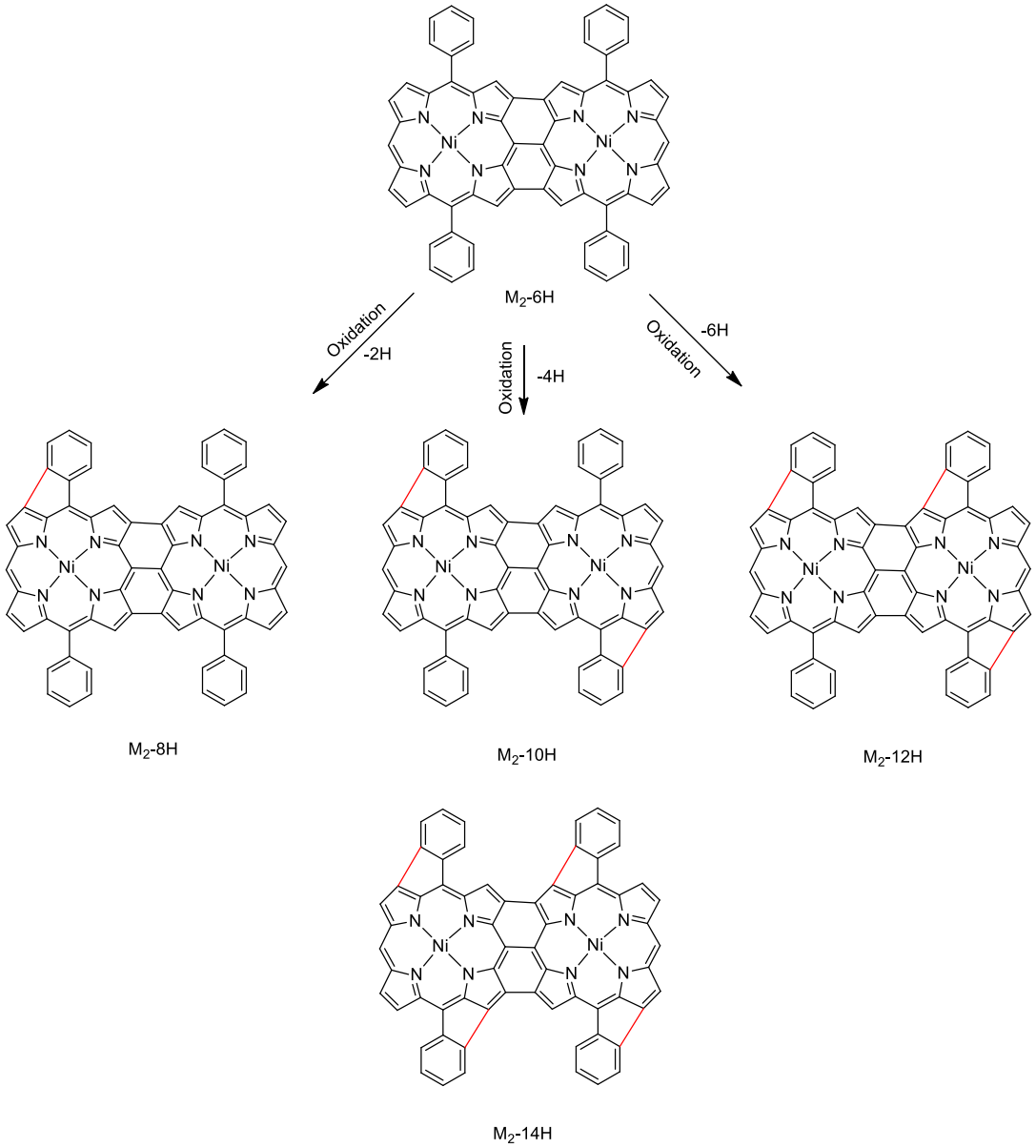

Scheme S3. Schematic of the dimeric triply linked NiDPP species formed during the oCVD reaction of NiDPP. The exact position of the unsaturations formed between the phenyl ring and the porphyrin macrocycles is still unclear and other structures are possible.

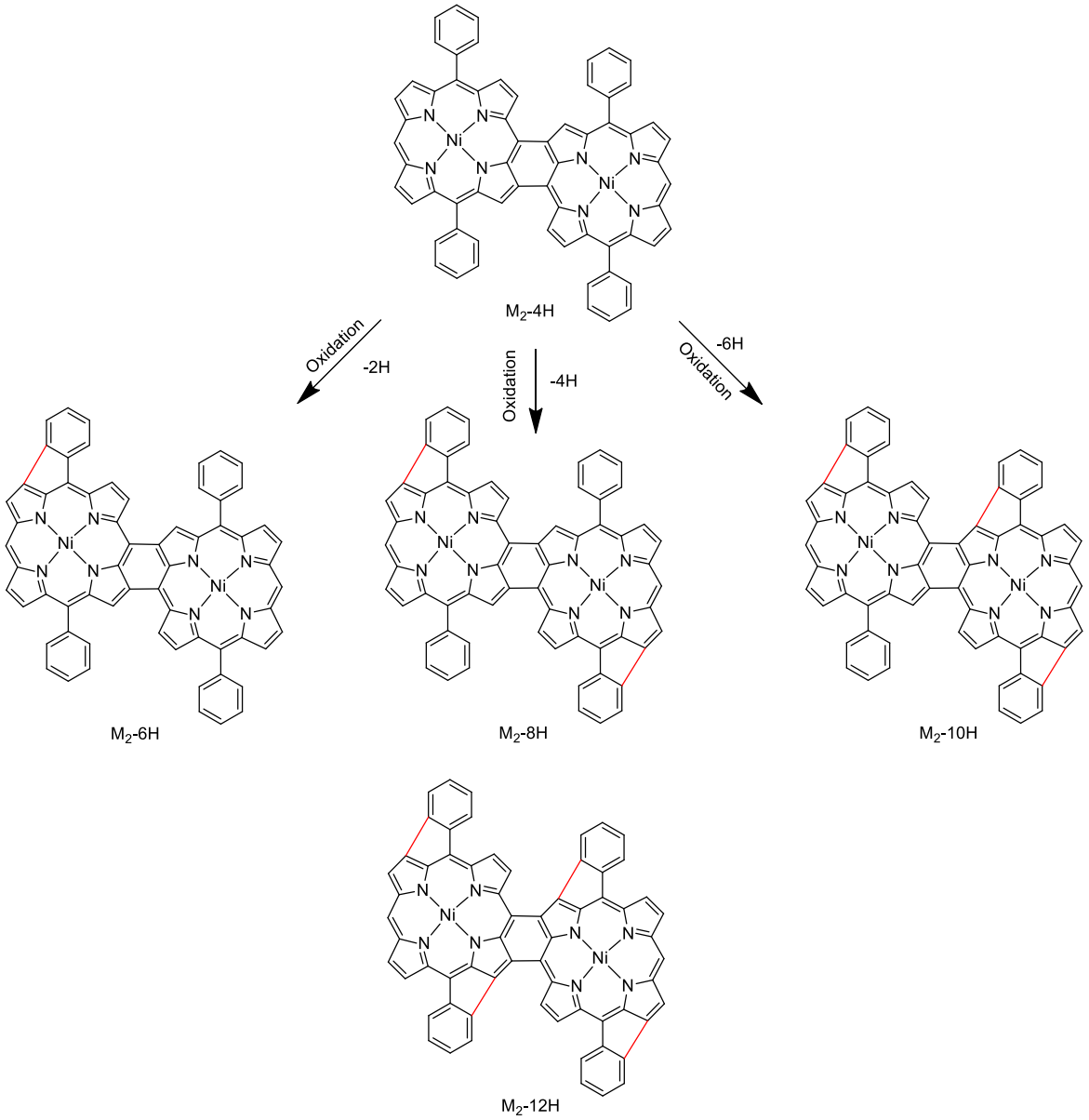

Scheme S4. Schematic of the dimeric doubly linked NiDPP species formed during the oCVD reaction of NiDPP. The exact position of the unsaturations formed between the phenyl ring and the porphyrin macrocycles is still unclear and other structures are possible.

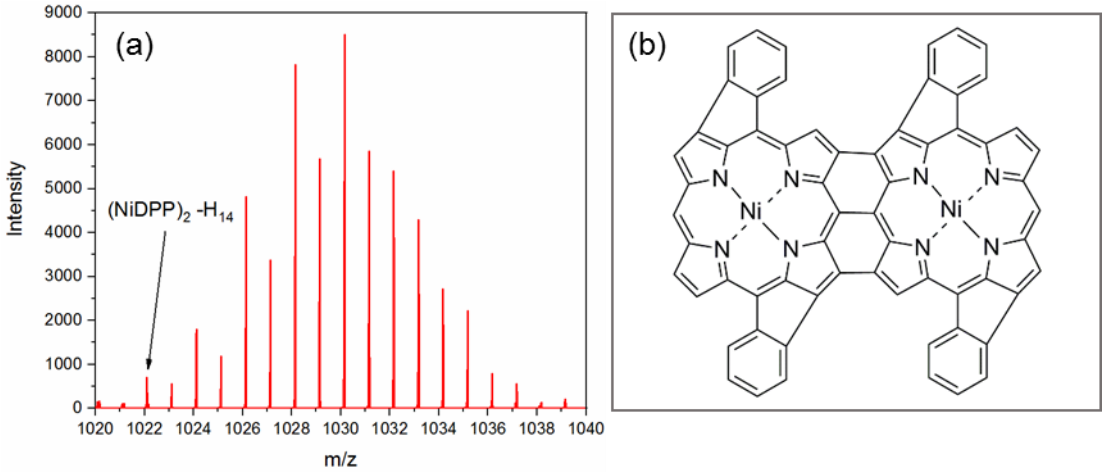

Figure S11. (a) AP-LDI-HRMS spectrum (dimer region) of the oCVD thin film deposited at 200°C. The signal related to the formation of the triply-fused porphyrin dimers with the four phenyl ring fused to the porphyrin core (m/z_{observed} 1022.099; $m/z_{calculated}$ 1022.098; mass error < 1ppm). (b) Scheme of a triply-fused porphyrin dimers with the four phenyl rings fused to the porphyrin cores (*trans* conformation). It is worth to note that the exact position of the intramolecular coupling reaction is still unclear and only pictorial. If the *cis* conformation is known to be favoured in the presence of electron withdrawing groups,[1] the absence of substituent at the position 10 and 20 of our porphyrin is likely to induce a different spin density yielding to a possibly different regioselectivity**.**

[1] Fukui, N; Lee, S.-K.; Kato, K.; Shimizu, D.; Tanaka, T.; Lee, S.; Yorimitsu, H.; Kim, D.; Osuka, A. Regioselective Phenylene-Fusion Reactions of Ni(ii)-Porphyrins Controlled by an Electron-Withdrawing *meso*-Substituent. *Chem. Sci.* **2016**, *7*, 4059-4066. https://doi.org/10.1039/C5SC04748J.

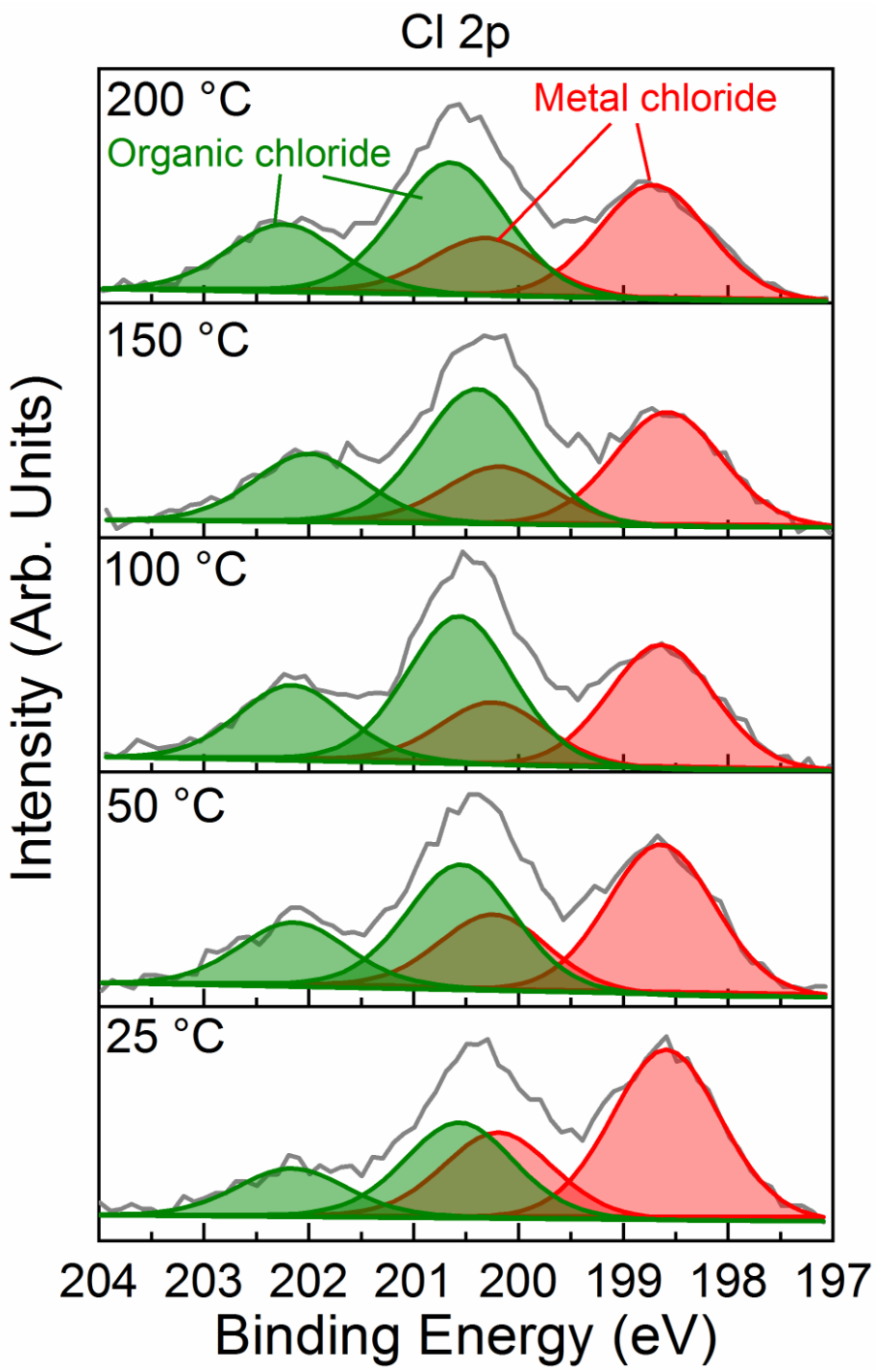

Figure S12. XPS curve-fitting of the Cl 2p core level for the oCVD thin films elaborated at different substrate temperatures. The organic chloride contributions (Cl $2p_{3/2}$ = ca. 200.8 eV and Cl $2p_{1/2}$ = ca. 202.4 eV) is depicted in green, alongside the metal chloride contributions (Cl $2p_{3/2}$ = ca. 198.7 eV and Cl $2p_{1/2}$ = ca. 200.3 eV) in red.